JOURNAL OF GEOPHYSICAL RESEARCH, VOL. 113, D22101, doi:10.1029/2008JD010072, 2008

Daily to submonthly weather and climate characteristics of the summer 1998 extreme rainfall over the Yangtze River Basin

Hongbo Liu,[1,2,3] Da-Lin Zhang,[2] and Bin Wang[1]

Received 5 March 2008; revised 14 July 2008; accepted 16 September 2008; published 20 November 2008.

[1] In this study, the daily to submonthly weather and regional climate characteristics associated with the extreme rainfall events over the middle to lower reaches of the Yangtze River Basin (YRB-ML) during the summer of 1998 are examined using the National Centers for Environmental Prediction/Department of Energy Reanalysis-2 data and a 54-day high-resolution (i.e., Δx = 4 km) simulation with a regional climate model (RCM). As verified against various observations, the RCM reproduces reasonably well the accumulated daily to biweekly rainfall events, their generation and subsequent evolution along the Meiyu front, and especially the rainfall events over the YRB-ML during the later stage of the 1998 floods. It is found that the early stage of the 1998 floods resembles in many aspects that occurred in normal years, except for a moister-than-climate state and stronger-than-normal low-level jets (LLJs) in Southeast China, whereas the later stage exhibits two abnormal height anomalies to the northeast and southwest of the YRB-ML, facilitating convergence of northeasterly and southwesterly flows along the Meiyu front. It is also found that the Meiyu front weakens in depth and intensity as it migrates northward across and then retreats to the YRB-ML, playing less important roles in rain production. Results show different daily to biweekly rainfall characteristics at the different stages, e.g., from eastward propagation to local generation of mesoscale convective systems and periodical rain production along the Meiyu front, most of which reach their maximum intensities over the YRB-ML during the morning to early afternoon hours. Results indicate that the northeasterly moisture supply enhances the production of steady heavy rain at the later stage of the 1998 floods. It is concluded that the West Pacific subtropical high and the Meiyu front control the general areas of rain production, the low-level moisture supply through LLJs and mesoscale disturbances determines whether or not sustaining flooding rains would occur, and what rainfall characteristics are at the daily to biweekly timescales.

Citation: Liu, H., D.-L. Zhang, and B. Wang (2008), Daily to submonthly weather and climate characteristics of the summer 1998 extreme rainfall over the Yangtze River Basin, *J. Geophys. Res.*, *113*, D22101, doi:10.1029/2008JD010072.

1. Introduction

[2] The middle to lower reaches region of the Yangtze River Basin (YRB-ML), located in eastern China, is one of the most climate-sensitive areas in East Asia. This basin receives quasi-steady heavy rainfall (i.e., Meiyu) during the meridional passage of well-known Meiyu-frontal systems that last typically 20 to 25 days, i.e., roughly from mid-June to mid-July [*Ding*, 1994]. The Meiyu front is characterized by weak temperature gradients but high equivalent potential temperature (θ_e) gradients due to strong meridional moisture contrasts, and large horizontal wind shear. However, during the growing season of 1998, two different heavy Meiyu rainy phases occurred over the YRB-ML: one on 12–30 June, and the other on 20–31 July, lasting for about 31 days. It was the heavy rainfall during the two phases, and additional rainfall in August at the upper reach of Yangtze River, that caused the unusual catastrophic flooding and inundation along the YRB in the summer of 1998 [*Tao et al.*, 1998], which was the most severe floods over the region since the year of 1954.

[3] The extreme Meiyu rainfall of summer 1998 has been extensively studied from its climatic background to its associated mesoscale processes. Previous studies revealed anomalous circulations and rainfall patterns during the warm season of 1998 as a result of significant changes in sea-surface temperature (SST) and snowfalls over the Tibet Plateau. Specifically, the summer of 1998 coincided with the weakening phase of El Niño-Southern Oscillation (ENSO), with an unusual amount of snowfall over the Tibet

[1] LASG, Institute of Atmospheric Physics, Chinese Academy of Sciences, Beijing, China.
[2] Department of Atmospheric and Oceanic Science, University of Maryland, College Park, Maryland, USA.
[3] Graduate University of Chinese Academy of Sciences, Beijing, China.

0148-0227/08/2008JD010072$09.00

Plateau during the previous cold season [*Lau and Weng*, 2001; *Huang et al.*, 1998; *Tao et al.*, 1998], and colder SSTs over the tropical West Pacific. Thus the West Pacific subtropical high (WPSH) was pushed to the south of its climate location as a result of less convective forcing near Philippine [*Sun and Ma*, 2001]. This facilitated the shift of major rainfall events southward compared to normal years. On the other hand, the anomalous intense snowfall decreased the land-sea thermal contrast and led to the weakening of the East Asian summer monsoon (EASM). Consequently, the monsoon circulation was maintained over southern and central China, providing a favorable background for the development of the Meiyu rainfall over the YRB-ML [*Chen*, 2001].

[4] Mesoscale observational and modeling case studies showed the importance of meso-β and meso-γ scale cloud systems in the generation of individual heavy rainfall events along the Meiyu front [e.g., *Bei and Zhao*, 2002] and also revealed the tropical origin of moisture supply as well as the positive feedback between the low-level jets (LLJs) and rainfall through condensational heating and intensification of local circulations [e.g., *Qian et al.*, 2004]. After analyzing different circulation patterns between the two Meiyu rainy phases, *Sun and Zhao* [2003] emphasized the important effects of cold air from higher latitudes on the development of the second phase heavy rainfall. *Ren and Wu* [2003], and *Ren et al.* [2004, 2007] attributed this second rainfall phase to the abrupt southward retreat of the WPSH and the adjustment of midlatitude circulations by the lower-level baroclinic eddies and the upper-level vorticity advection associated with the South Asian High.

[5] Because of the extensive rainfall over the YRB-ML, regional climate models (RCMs) have also been used to study the daily to subseasonal climate characteristics during the summer of 1998. For example, *Wang, Y.-Q., et al.* [2003], *Lee et al.* [2004] and *Leung et al.* [2004] all reproduced to some extent the observed large-scale circulations and the monthly evolution of summer monsoon rainfall with their RCMs. However, these simulation studies primarily examined the ability of RCMs to reproduce warm-season regional climate with extreme rainfall in East Asia. In addition, *Gao et al.* [2006], *Tang et al.* [2006] and *Xue et al.* [2007] found that the use of higher resolutions of an RCM would improve the simulation of precipitation at weekly to subseasonal timescales.

[6] While the previous studies provided some useful understanding of the general circulations or some mesoscale episodes associated with the summer 1998 heavy rainfall, little work has been done to compare the large-scale mean circulation characteristics during the two rainy phases and the transition between. In particular, the mechanisms by which the extreme rainfall occurred during the two rainy phases still remain poorly understood. Moreover, the second rainy phase was not well reproduced by the previous modeling studies. Thus the objectives of the present study are to (1) demonstrate the RCM's capability of reproducing the major rainfall events occurring over the YRB-ML during the summer of 1998; (2) examine the pertinent daily to submonthly weather and regional climate characteristics; and (3) explore different rainfall-generating mechanisms and larger-scale flows during the two heavy rainy phases. This will be achieved through diagnoses of the National Centers for Environmental Prediction/Department of Energy (NCEP/DOE) Reanalysis-2 (R-2) data and the use of a 54-day high-resolution RCM simulation of the major flood events occurring during the summer of 1998. The transition between the two rainy phases will also be studied.

[7] The next section provides an overview of the large-scale circulations and anomaly fields with respect to climate as well as the observed rainfall characteristics during the period of 12 June to 31 July 1998. Section 3 describes the RCM used, and section 4 shows the model verification against the R-2 analysis and station observations. Section 5 presents analyses of the large-scale mean thermodynamic and flow structures as well as precipitation characteristics at daily to biweekly timescales. A summary and concluding remarks are given in the final section.

2. Overview

[8] Because the evolution of the East Asian summer monsoonal rainfall, including the Meiyu rainfall, is closely related to that of the WPSH and midlatitude traveling waves, Figure 1 shows the 500-hPa mean geopotential height and temperature fields during the two rainy phases and a transition period in between encompassing a total of 50 days (i.e., from 12 June to 31 July 1998), whereas Figure 2 compares the submonthly flow anomalies with respect to the corresponding 20-year (i.e., 1979–1998) mean fields in the upper, middle and lower troposphere between the two rainy phases; they are all based on the 6 hourly, 2.5°-resolution NCEP/DOE R-2 data.

[9] It is apparent from Figure 1 that the large-scale midlatitude disturbances and the WPSH at 500 hPa have undergone significant adjustments during the 50-day period. During the first rainy phase, a well-defined trough axis, though weakening southwestward, extended from central to northeastern China and then northwestward into central Russia, with a "blocking" high located to the southwest (Figure 1a). This wave pattern allowed the polar cold and dry air to be intruded into the central-east portion of China (i.e., YRB-ML, shown by an interior box in all horizontal figures). In contrast, the WPSH, centered over the central Pacific Ocean, dominated part of South China such that the tropical warm and moist air could be transported to the YRB-ML by southwesterly flows. As a result, a near-west-east-oriented Meiyu front, to be shown in section 5, was formed along the YRB-ML where the warm-moist and cold-dry air masses met, providing favorable conditions for the development of quasi-stationary rainfall along the frontal zone (see Figure 3). During the transition phase (i.e., 1–19 July), the northwestern portion of the WPSH was pushed to the YRB-ML and even to northern East Asia, with a weak trough to the west (Figure 1b). Little evidence of quasi-geostrophic ascent could be seen in this simple tropical air flowing over the eastern half of China, Korea and Japan. So, central East China experienced mostly hot and humid weather conditions with much less rainfall as in normal years (see Figure 3). During the second rainy phase, northern China and the YRB-ML were dominated by weak west-northwesterly flows behind a trough axis located over the Korean peninsula, as the WPSH was retreated to South China Sea (SCS, see Figure 1c). Clearly, the quasi-geostrophic influences of both the trough and WPSH on the YRB-ML's biweekly

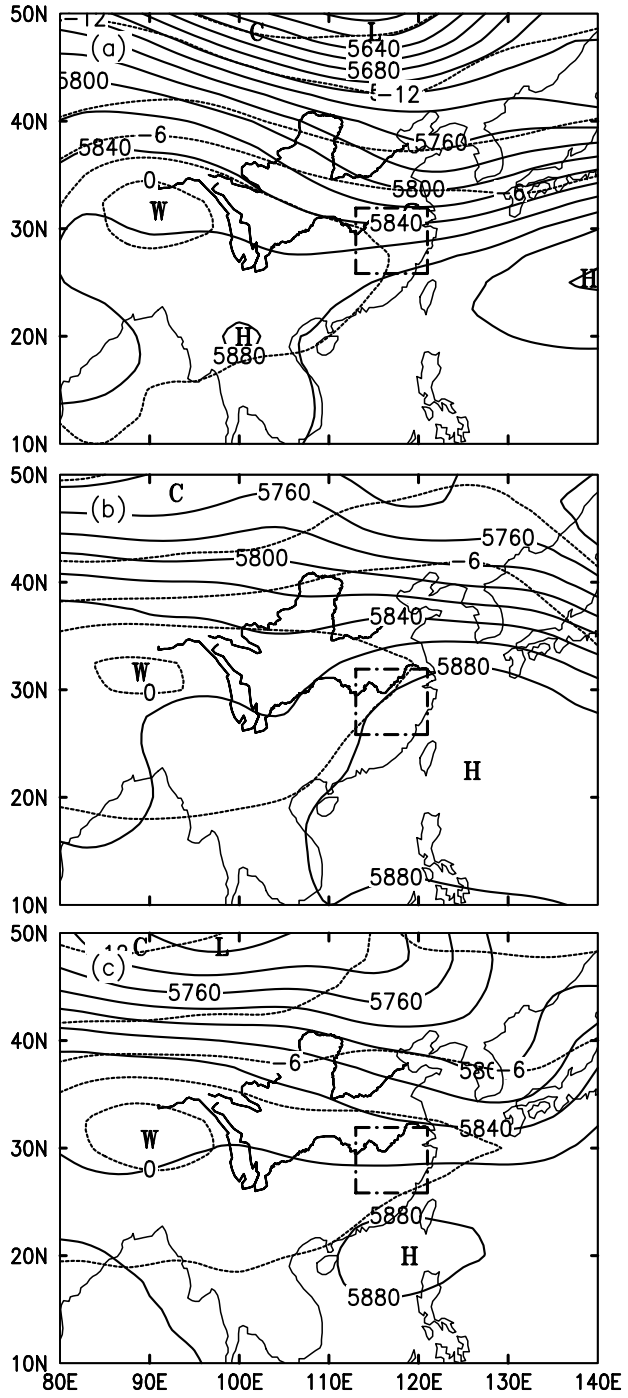

Figure 1. The NCEP/DOE reanalysis (R-2) of the 500-hPa geopotential height (solid lines, every 20 m) and temperature (dashed lines, every 3°C) that are averaged during the period of (a) 12–30 June 1998, (b) 1–19 July 1998, and (c) 20–31 July 1998. The interior box (dot-dashed lines) denotes the YRB-ML region (i.e., 26–32°N, 113–121°E).

weather were much weaker than, and the origin of moisture differs from those during the first rainy phase.

[10] Since any extreme rainfall event must be supported by anomalously favorable larger-scale conditions, we examine the associated large-scale flow anomalies at the biweekly to submonthly timescales, and compare them between the two rainy phases. It is apparent from Figures 2a and 2b that North China during the first rainy phase was characterized by northerly flow anomalies that increased upward in magnitude and coverage; the relatively cold northerlies had reached the YRB-ML. There were a strong cyclonic wind anomaly to the north and an anticyclonic wind anomaly over SCS, which are consistent with the 19-day averaged height anomaly field. In the lower troposphere, the dominant features were southwesterly anomalous flows and a large anticyclonic circulation anomaly over SCS and West Pacific (Figure 2c), thereby transporting more warm-humid air northward into the YRB-ML. Their convergence with the weakest anomalous flows along the Meiyu front could be seen at 850 hPa along the YRB-ML, indicating the normal location of the Meiyu front over the region where the southwesterly moist air is lifted for latent heat release.

[11] By comparison, the large-scale flows during the second rainy phase showed a deep, intense cyclonic circulation anomaly over the Korean peninsula which tended to transport the moist air mass, albeit slightly colder, over Sea of Japan and Yellow Sea to the YRB-ML through its northeasterly to northerly perturbation flows in the lower troposphere (Figures 2e–2g). A similar cyclonic circulation, though much weaker than its anomaly field, did appear in the lower troposphere, as partially shown in Figure 8f. This moist north-to-northeasterly anomaly from the back of the YRB-ML met with the low-tropospheric southwesterly perturbation flows associated with an anticyclonic circulation anomaly over SCS (Figure 2g), forming a west-east-oriented moisture convergence zone over the region. It should be noted that the negative height anomaly over the Korean peninsula and the positive height anomaly over SCS were both abnormal compared to the general climate in East Asia during this period (see Figures 2e–2g). As will be seen in section 5 (cf. Figures 8a and 8c), this convergence zone differs in several aspects from the typical "deep" Meiyu frontal zone in the first rainy phase.

[12] Figures 2c and 2g compare the water vapor anomalies at 850 hPa between the two rainy phases. Evidently, the YRB-ML exhibited a moister-than-climate state along a 500-km width zone to the south of the Meiyu front with greater than 1- and 2-g kg^{-1} positive moisture anomalies during the first (Figure 2c) and second (Figure 2g) rainy phase, respectively. The column-integrated moisture flux anomalies showed that these positive moisture anomalies originated from SCS and West Pacific, and then converged toward the south of the YRB-ML through the subtropical anticyclonic circulation anomaly. They were much greater in magnitude and coverage during the second than those during the first rainy phase (cf. Figures 2d and 2h), because the YRB-ML would be under the control of the WPSH in normal years during the second phase. The anomalous moisture transport from Yellow Sea and Sea of Japan into the YRB-ML is also evident during the second rainy phase (Figure 2h). The results indicate the importance of anomalous moisture sources in facilitating the development of extreme rainfall over the YRB-ML during the summer of 1998. This finding could be considered as a supplement to the moisture budget analysis of *Ding and Hu* [2003] for the extreme rainfall events.

[13] It is apparent from the above analysis that despite some dynamical and thermodynamic differences between

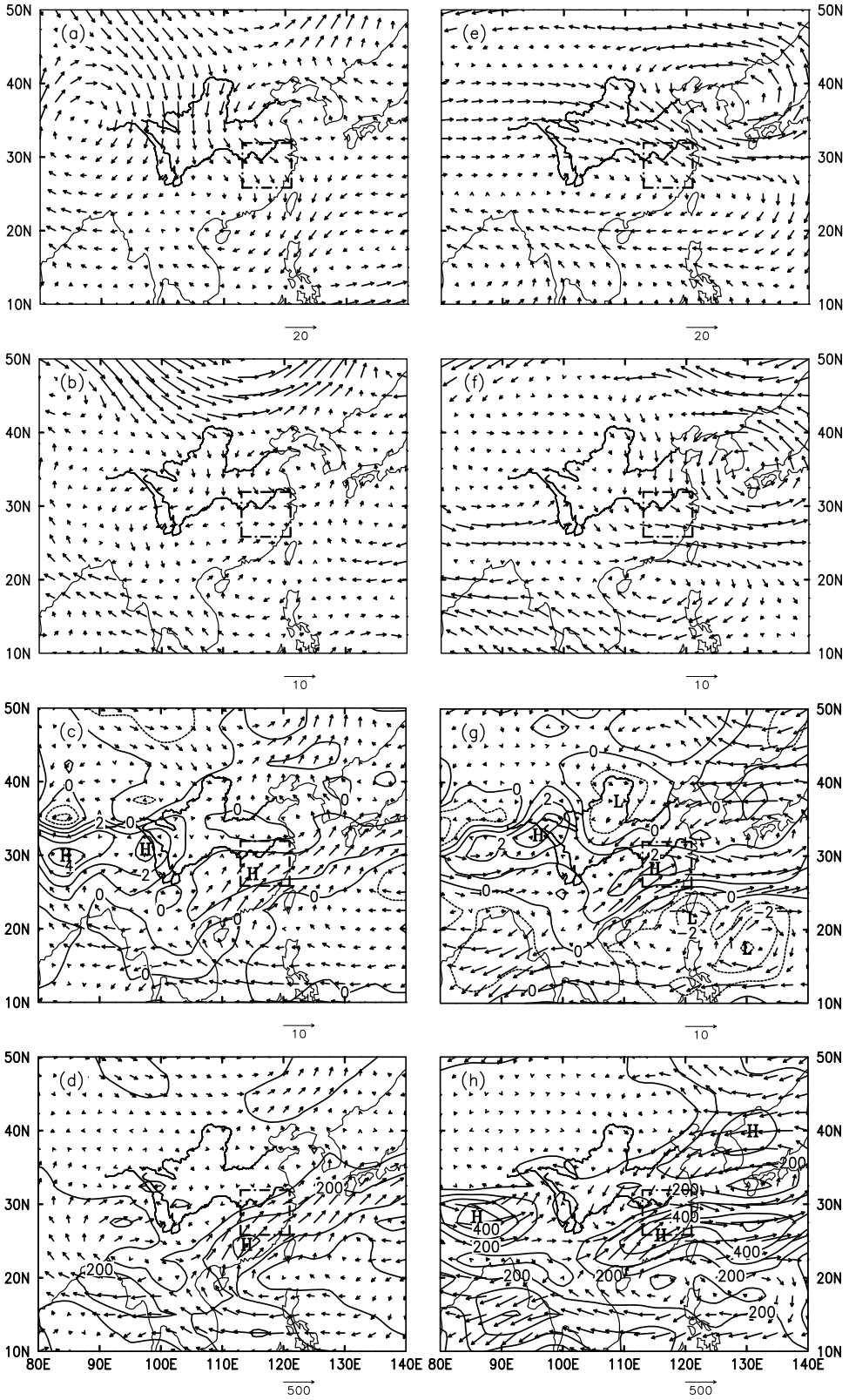

Figure 2. (a, e) Anomalies of horizontal wind vectors (m s^{-1}) at 200 hPa, (b, f) anomalies of horizontal wind vectors (m s^{-1}) at 500 hPa, (c, g) anomalies of specific humidity (solid lines, every 1 g kg^{-1}) and horizontal wind vectors (m s^{-1}) at 850 hPa; (d, h) anomalies of column-integrated moisture flux (every 100 kg $m^{-1}s^{-1}$) for the period of (left column) 12–30 June 1998 and (right column) 20–31 July 1998. They are obtained by subtracting the 20-year average (i.e., from 1979 to 1998) using the NCEP/DOE R-2 reanalysis data. The interior box (dot-dashed lines) denotes the YRB-ML region (i.e., 26–32°N, 113–121°E).

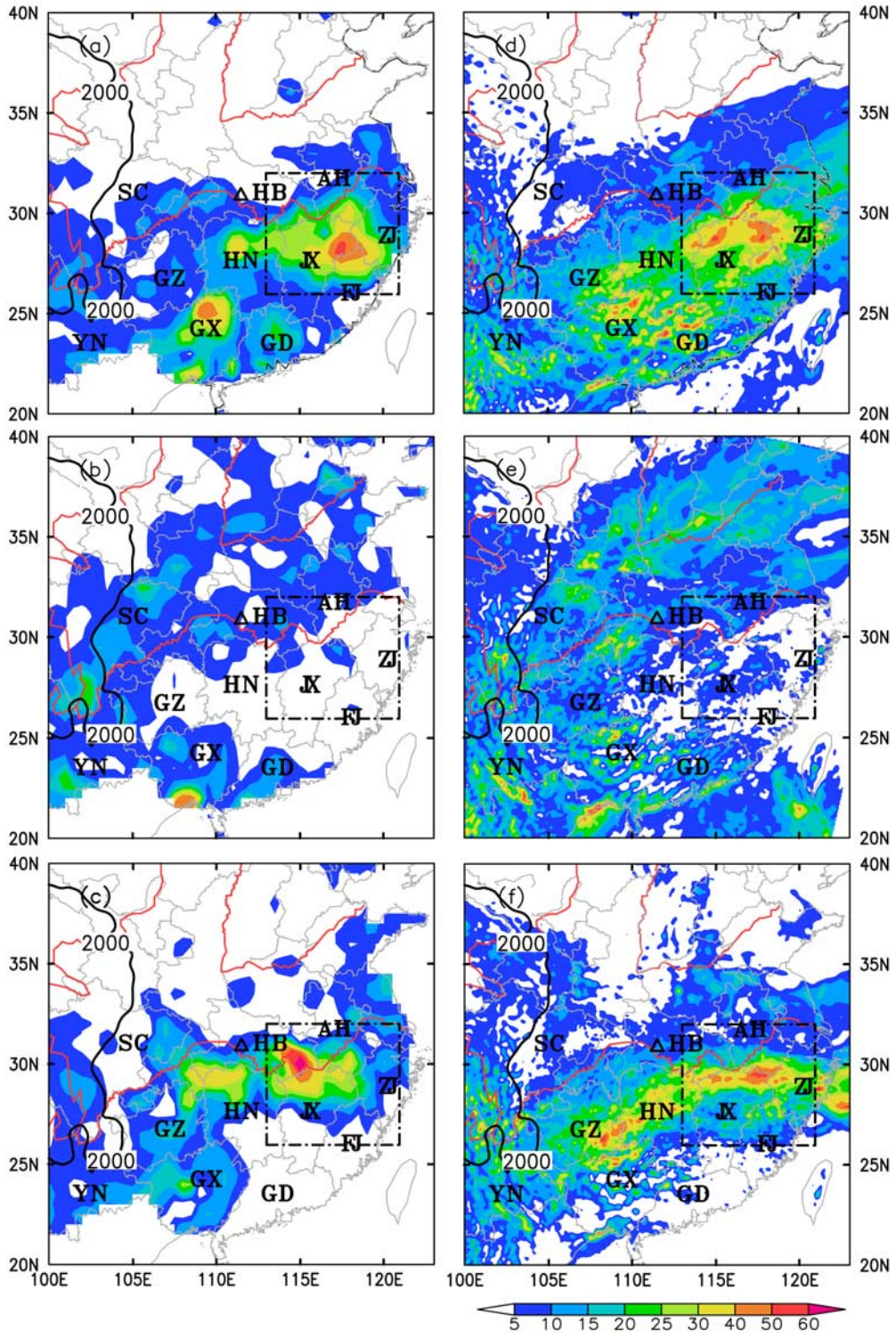

Figure 3. Horizontal distribution of the averaged daily rainfall rates (mm d^{-1}) from (left column) the station observations and (right column) the model-domain 2 over East China for the period of (a, d) 12–30 June 1998; (b, e) 1–19 July 1998; and (c, f) 20–31 July 1998. Provincial boundaries (light lines) and Yangtze and Yellow River (in red) are shown. SC, Sichuan; GZ, Guizhou; YN, Yunnan; AH, Anhui; HB, Hubei; HN, Hunan; JX, Jiangxi; ZJ, Zhejiang; FJ, Fujian; GX, Guangxi; GD, Guangdong. The interior box (dot-dashed lines) denotes the YRB-ML region (i.e., 26–32°N, 113–121°E). The solid black contour denotes the distribution of 2000-m terrain elevation, and a triangle is used to indicate the location of the Yichang hydrological station.

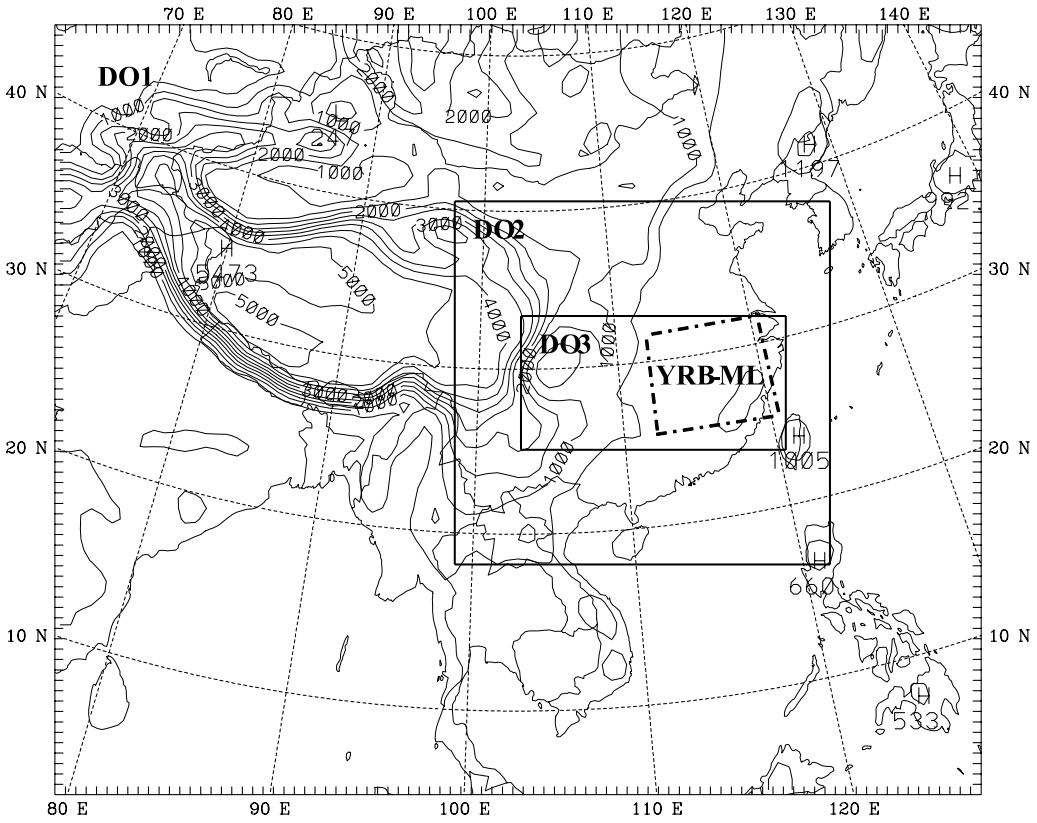

Figure 4. The model triply nested-grid domains and the model topography at intervals of 500 m. The interior box (dot-dashed lines) denotes the YRB-ML region (i.e., 26–32°N, 113–121°E).

the two rainy phases, the southward transport of cold and dry air masses aloft from higher latitudes combined with the northward transport of tropical warm and moist air masses in the lower troposphere helped destabilize the atmospheric columns, favoring the generation of persistent convective rainfall at the timescales of individual phases. This appeared to be particularly true during the second rainy phase.

[14] The distributions of the accumulated precipitation during the three different phases are given in Figure 3, which were obtained from 606 hourly rain-gauge stations, all subjected to critical quality control [*Yu et al.*, 2007a], at roughly 1.0° resolution in East China. (A comparison of the observed rainfall to the model-simulated, i.e., between Figures 3a–3c and 3d–3f, will be discussed in section 4.) Figure 3a shows that the Meiyu frontal rainfall was distributed along a west-east-oriented belt of 400–500 km in width to the south of Yangtze River with a maximum rainfall rate of over 50 mm d^{-1} at the eastern Jiangxi (JX) Province. Widespread weak mean rainfall, associated mostly with the surface-heating generated thunderstorms, also occurred over most of South China, except over the northern Guangxi (GX) Province where the passages of several mesoscale convective systems (MCSs) produced considerable rainfall with an average rate of over 40 mm d^{-1}. The local topography appeared to play an important role in uplifting the high-θ_e air in the monsoonal flows for the generation of heavy rainfall in GX, and of the general rainfall belt from southern GX to the western portion of the Meiyu front (cf. Figures 3 and 4). The topographical effects on the initiation of deep convection will be shown in section 5. The heavy rainfall was shifted north- and westward (to the upper reach of Yangtze River) after 26 June, causing the passage of the first flood peak on 2 July at the Yichang hydrological station, located at 111.5°E in Hubei Province (HB) [*Chen et al.*, 1998]. As the WPSH was pushed northwestward during the transition phase, South China experienced little rainfall because of the presence of unfavorable quasi-geostrophic conditions (cf. Figures 1b and 3b). Instead, the major rainfall belt associated with the Meiyu front, albeit much weaker than earlier, was displaced northward into the Yangtze - Yellow River basin, like that occurring in normal years. Within this period, the upper reach of Yangtze River also experienced steady heavy rainfall, leading to the second flood peak passed by Yichang on 17 July [*Chen et al.*, 1998]. The second rainy phase exhibited a more west-east elongated belt that extended from the upper to middle and lower portion of Yangtze River, with a maximum rainfall rate of over 70 mm d^{-1} over the southeastern HB, causing the third flood peak at Yichang on 24 July [*Chen et al.*, 1998]. This rainfall belt was produced along the retreating Meiyu front, to be shown in section 5, which was abnormal because the Meiyu front often diminishes as it advances northward.

3. Model Description

[15] In this study, the nested-grid, nonhydrostatic version V3.7.2 of the Pennsylvania State University-National

Table 1. Model Grid Size and Terrain and Land Use Design for Three Domains

Domains	Grid Size (km)	Dimension (x, y)	Terrain and Land Use
Domain1 (DO1)	36	180 × 150	5 min (~9 km)
Domain2 (DO2)	12	208 × 217	2 min (~4 km)
Domain3 (DO3)	4	424 × 256	2 min (~4 km)

Center for Atmospheric Research (PSU-NCAR) mesoscale model (i.e., MM5) is used as an RCM to study the daily to submonthly weather and climate characteristics of the Summer 1998 extreme rainfall events. The MM5, with different physics options and different initial and lateral boundary conditions, have been used by *Leung et al.* [2004] and *Lee et al.* [2004] to study the 1998 warm season rainfall as an RCM problem.

[16] The model water cycles used for this study include (1) a simple ice microphysics scheme for grid-scale precipitation with the prognostic equations for cloud water, cloud ice, rain water and snow [*Zhang*, 1989; *Dudhia*, 1989]; (2) the newest version of the Kain-Fritsch (KF2) convective parameterization scheme for subgrid scale convection including the effects of shallow convection [*Kain*, 2004]; (3) the Eta model's Mellor-Yamada planetary boundary layer (PBL) scheme [*Janjić*, 1994]; (4) a long- and short-wave radiation scheme which interacts with the atmosphere, cloud, and land surface [*Dudhia*, 1989]; and (5) the NCEP-Oregon State University-Air Force-Hydrologic Research Lab (NOAH) land surface model [*Chen and Dudhia*, 2001a, 2001b].

[17] Figure 4 shows the two-way interactive, triply nested-grid domains with a ratio of 3. Domain 1 (DO1) covers the most part of Asia, including its surrounding oceans, with a grid size of 36 km. Domain 2 (DO2) includes the central and eastern half of China with its western boundary at eastern Tibet Plateau, while domain 3 (DO3) covers all the YRB-ML, where the two extreme rainfall phases occurred (cf. Figures 4 and 3), with the finest grid size of 4 km; See Table 1 for more details. Note that because of the two-way interactive procedures used, the model outputs show little differences between domains 2 and 3, particularly after they are temporally or spatially averaged. There are 34 σ-levels in the vertical; they are 1.00, 0.995, 0.99, 0.98, 0.97, 0.96, 0.94, 0.92, 0.90, 0.88, 0.84, 0.80, 0.76, 0.72, 0.68, 0.64, 0.60, 0.56, 0.52, 0.48, 0.44, 0.40, 0.36, 0.32, 0.28, 0.24, 0.20, 0.16, 0.12, 0.08, 0.06, 0.04, 0.02, and 0.00, which give 33 σ-layers. The model top is set at 50 hPa.

[18] The model initial and lateral boundary conditions are taken from the NCEP's 6 hourly R-2 data. The initial soil variables are from the European Centre for Medium Range Weather Forecasts (ECMWF) 40-Year reanalysis (ERA-40), which are nudged toward the observed screen-level temperature and humidity. The SST field at individual grid points is obtained by linearly interpolating in both time and space the Reynolds weekly SST at 1°-resolution [*Reynolds and Smith*, 1994].

[19] The model is initiated at 0000 UTC 8 June 1998 and then continuously integrated to 1800 UTC 31 July 1998. The first 4-day integrations are treated as the model spin-up, so they are not used for the model analysis. Like *Wang, Y.-Q., et al.* [2003] and *Lee et al.* [2004], we adopt a buffer zone of about 1000 km (30 grid intervals) along each outermost lateral boundary so as to keep the incoming large-scale flows reasonably defined. During the 54-day simulation period, the lateral boundary conditions and SST are updated every 6 hours, and the model results are output hourly for the sake of analyzing the daily to submonthly weather and climate characteristics during the three different phases.

4. Model Verification

[20] It is well accepted that for RCM simulations the upper-level circulations are primarily determined by the outmost lateral boundary conditions while the bottom surface forcings tend to modulate precipitation patterns and some meteorological variables in the lower troposphere [*Giorgi*, 1990]. Thus, as expected, the MM5 could reproduce well the 3D wind and geopotential height fields at the upper levels (not shown), as verified against the NCEP/DOE reanalysis. So in this section we focus more on the verification of the simulated precipitation and low-level fields during the two rainy phases and the transition phase in between.

[21] In general, MM5 simulates reasonably well the distribution and magnitude of accumulated rainfall during the three phases (cf. Figures 3a–3c and 3d–3f). For example, the model reproduces the widespread rainfall in the southern half of China with two heavy rainfall regions: one in the northeastern JX and the other in the northern GX Province during the first rainy phase, the northward shift of the Meiyu frontal rainfall with trailing light rainfall over the YRB-ML and little rainfall over southeastern China during the transition phase, and the west-east-elongated rainfall belt along Yangtze River during the second rainy phase. However, significant errors in the locations of heavy rainfall can be noted, particularly during the second rainy phase. That is, a different orientation of the rainfall belt from the observed over GX and northern HN is simulated, and the heavy rainfall center near the city of Wuhan, HB is missed (cf. Figures 3c and 3f). It is found that the latter was generated by a quasi-stationary MCS, fed by converging high-θ_e air associated with a pressure low over Southwestern China and the other low over Yellow Sea [*Zhang et al.*, 2002], that could not be well reproduced by most numerical models due to the lack of mesoscale predictability beyond a few days. Nevertheless, this event has little impact on the submonthly weather and climate characteristics after temporal and spatial averages. It should be mentioned that none of the previous studies [e.g., *Wang, Y.-Q., et al.*, 2003; *Lee et al.*, 2004; *Leung et al.*, 2004] was able to reproduce this west-east-elongated rainfall belt properly during this rainy phase. Our more reasonable simulation could be attributed to the use of the Kain-Fritsch scheme and high resolution; this will be explored in detail in a forthcoming paper. It should also be mentioned that the simulated rainfall exhibits many more (realistic) smaller-scale features than the observed, some of which are associated with local topography due to the use of 4-km resolution terrain data (see Table 1).

[22] We compare in Figure 5 the time series of the area-averaged daily rainfall rates over the YRB-ML between the

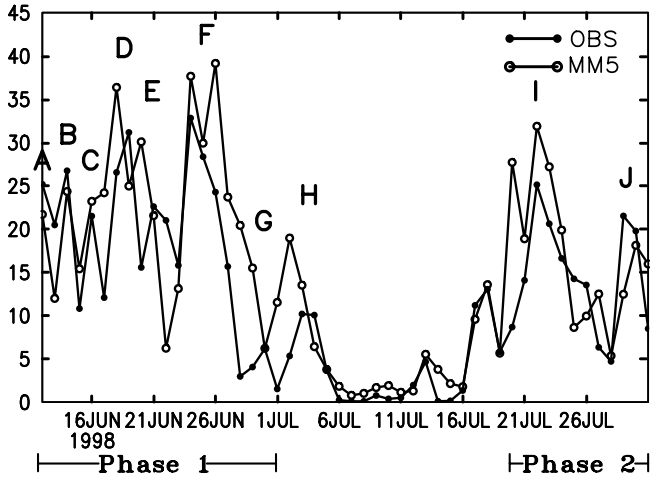

Figure 5. Time series of the daily rainfall rates (mm d^{-1}) averaged over the YRB-ML region (26–32°N, 113–121°E) from the station observations (solid circle) and the model-domain 3 (hollow circle) during the period of 12 June to 31 July 1998. Letters "A" to "J" denote the passage of major precipitating weather systems or events over the YRB-ML region (see Figure 10 for more detail).

observations and simulation. Although the first rainy phase produced a bulk of the total accumulated rainfall (through events A–F), the observed catastrophic flood disaster did not take place until the highest rainfall rate occurred on 22 July (i.e., during the second phase). In general, the model reproduces most of the observed rainfall peaks (i.e., A–F, H, I and J) during the two rainy phases, and light rainfall during the transition phase (i.e., 5–16 July), albeit with greater magnitudes on a few days. On average, the correlation coefficient between the simulation and observations is 0.78, indicating that the simulated rainfall events are reasonable and with the model verifications that follow, the associated data are suitable for process studies at daily to submonthly timescales.

[23] Figure 6 compares the time evolution of the high relative humidity (i.e., RH > 70%), as a proxy for rainfall, and the meridional winds at 850 hPa between the model simulation and the R-2 analysis. In general, MM5 reproduces the distribution of both variables in pattern and magnitude, except that the simulated meridional wind is about 2 m s^{-1} larger than that in the R-2 reanalysis during some time windows. The higher wind intensity appears to be reasonable when considering that the model resolution is much higher than that of the reanalysis. Obviously, the sustained rainfall occurs at the interface between the advancing tropical and retreating polar air masses, so this interface represents the northern end of the EASM in East China. The Meiyu season in 1998 begins with a quasi-stationary rainbelt located between 25–30°N and a southerly wind of greater than 8 m s^{-1}, which are similar to those in normal years. The Meiyu front moves northward on 26 June under the influence of the EASM, shifting the heavy rainbelt away from the YRB-ML. As the strong southerly monsoonal flows push the rainbelt beyond 35°N after 9 July, the frontal rainfall begins to weaken. This weakening appears to be caused partly by the limited meridional extent the monsoonal flow could reach, and partly by the reduced energy supply due to the convective development upstream of the YRB-ML (e.g., in GD, and GX). Note the periodical rainfall centers with enhanced southerly winds that, as will be seen in Figure 10, are associated with sustained MCS-complexes along the Meiyu front. Of significance is that as the Meiyu frontal rainfall diminishes after 18 July, the northerly flows quickly dominate over the northern region of the YRB-ML, so a new rainbelt develops and initiates the second rainy phase along the YRB-ML. It lasts for more than 10 days with stronger northerly flows than those occurring during the first phase.

[24] Figure 7 compares the time series of the area-averaged maximum and minimum (2-m) surface temperatures over the YRB-ML from the station observations to the simulated. The simulated (2-m) surface temperatures are calculated, following *Wang, Y.-Q., et al.* [2003], by averaging the air temperature at the lowest model level (i.e., σ = 0.9975) and the ground temperature. A general increase in the surface temperature can be seen, which is consistent with the surface warming trend toward the middle summer, except for the second rainy phase. Pronounced fluctua-

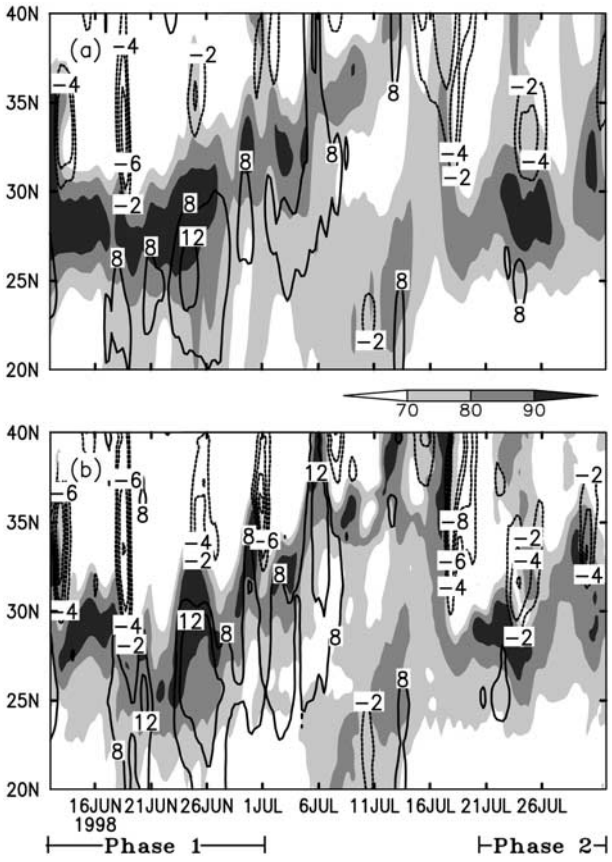

Figure 6. Time-latitude cross-section of 850-hPa meridional winds (m s^{-1}), contoured for southerly winds (solid lines; 8, and 12 m s^{-1}) and northerly winds (dotted lines; −2, −4, −6, and −8 m s^{-1}), and relative humidity (greater than 70% is shaded at intervals of 10%) zonally averaged across the YRB-ML (i.e., 113–121°E) from (a) R-2 reanalysis and (b) the model-domain 2 during the period of 12 June to 31 July 1998.

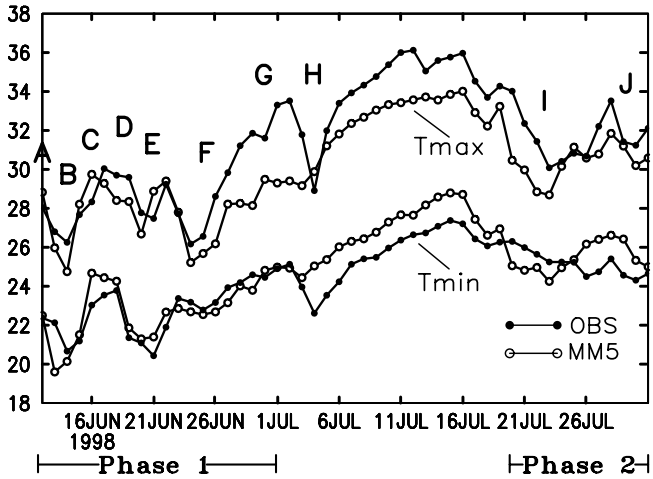

Figure 7. As in Figure 5 but for the maximum and minimum surface (2-m) temperatures (°C) from the observations (solid circle) and the model-simulated in domain 3 (hollow circle) during the period of 12 June to 31 July 1998.

tions in both the maximum and minimum temperatures are present, with the colder surface air coinciding closely with the periodical rainfall centers (cf. Figures 6b and 7). This coldness is clearly caused by the rainfall cooling and cloud shading effects. Unlike the first rainy phase, the decreasing trend during the second phase could not be fully explained by rainfall-cooling and cloud-shading effects. As will be seen in the next section, this appears to be affected partly by the cold air advection from the north, which differs from the retreating polar air mass scenarios associated with the Meiyu frontal systems. Surface temperatures exhibit larger diurnal differences (about 10°C) during the transition phase than those (about 7–8°C) during the rainy phases, with the smallest differences (about 5–6°C) during the periodical heavy rainfall periods (cf. Figures 6a and 7).

[25] In general, the model reproduces well the time evolution and trends of the observed maximum and minimum surface temperatures. Their general magnitudes during most of the rainy periods are also reasonably reproduced. However, there are some cold and warm biases, respectively, in the simulated maximum and minimum temperatures during the transition period. These biases could be attributed partly to the sparse observations over the mountainous regions that cover a sizeable portion of the YRB-ML, and partly to the systematic ways (or errors) to estimate the surface temperatures [e.g., *Dickinson et al.*, 1993; *Wang, Y.-Q., et al.*, 2003]. The coldest bias of 4.5°C occurs between event G and event H, which appears to be related to some overpredicted rainfall that is not present in the observations (cf. Figures 7 and 5).

5. Daily to Submonthly Characteristics

[26] After showing the RCM's ability to reproduce many observed features, we may use the simulation results to study more detailed three-dimensional structures and daily to submonthly characteristics of regional climate/weather over the YRB-ML. First, Figure 8 shows the three-dimensional mean structures of the Meiyu front and the mean larger-scale environments for the three different phases. There are two common features during the three phases that are important to be mentioned: a branch of organized southwesterly flows of high-θ_e air into the YRB-ML, and a low-level cyclonic circulation in eastern SC (Figures 8d–8f). The first rainy phase is characterized with large θ_e gradients (i.e., 20 K between 29–34°N or 4×10^{-2} K km^{-1}) but small temperature gradients (i.e., less than 5×10^{-3} K km^{-1}) below 400 hPa over the YRB-ML (Figure 8a), which are typical features of a Meiyu front [*Ding*, 1994]. Figure 8d shows that the Meiyu front separates the subtropical high-θ_e air mass from the dry polar air mass, and acts like a barrier for the low- to mid-tropospheric southwesterly flow to ascend (cf. Figures 8d and 9a), as indicated by marked gradients in wind speed. The convergent southwesterly flows account for widespread rainfall as the Meiyu front moves northward during this period (cf. Figures 3, 5, and 6). Thus, if the Meiyu front is defined herein as the northern end of subtropical air with the largest θ_e gradient, it would be located near 29, 37, and 30°N for the first, transitional and second phases, respectively (cf. Figures 8 and 9). The subtropical high-θ_e surface of 356 K in the PBL, and near-upright θ_e-surfaces in the vertical suggest the generation of predominately convective rainfall during the first rainy phase (Figure 8a), which is consistent with the development of the observed heavy rainfall over the YRB-ML. The resulting latent heat release, typically peaked in the middle to upper troposphere, facilitates the northeasterly flow to converge aloft with the southwesterly flow along the front (Figure 9a). Note the strong temperature gradients behind the front in the upper troposphere that are caused by the steady cold advection from higher latitudes and then enhanced by the heating-induced convergence (cf. Figures 2a, 8a and 9a).

[27] During the transitional phase, the Meiyu front becomes weaker and shallower as it advances northward to 37°N (see Figures 8b and 8e). Unlike the deep, upright frontal structures during the early season, it is somewhat "distorted" with lesser baroclinic forcing (cf. Figures 8a and 8b). In addition, the northward transport of subtropical high-θ_e air occurs in a channel that is much narrower and slightly weaker than that during the first rainy phase (cf. Figures 8d and 8e). As a result, weak, but notable, convergence occurs along the front, producing significant rainfall to the north of the YRB-ML (see Figures 3b and 3e). Although the YRB-ML is distributed with the subtropical high-θ_e air mass, there is little lifting to release the associated potential instability due to the dominant control of the WPSH (cf. Figures 1b, 8b, 8e and 9b).

[28] The second rainy phase is characterized by a weak and shallow Meiyu frontal zone in the lowest 100 hPa with near-symmetric distribution of high-θ_e air on both sides and the peak values over the YRB-ML (Figure 8c). In particular, the high-θ_e values to the north have increased 14–18 K during the past one month, due partly to the transport of moist air from Yellow Sea and Sea of Japan by a weak, quasi-stationary extratropical cyclone over the Korean peninsula (cf. Figures 8c, 8f, 9c and 2e–2f), and partly to the surface moisture fluxes associated with the precipitation that occurs during the transition period (cf. Figures 3e and 8c).

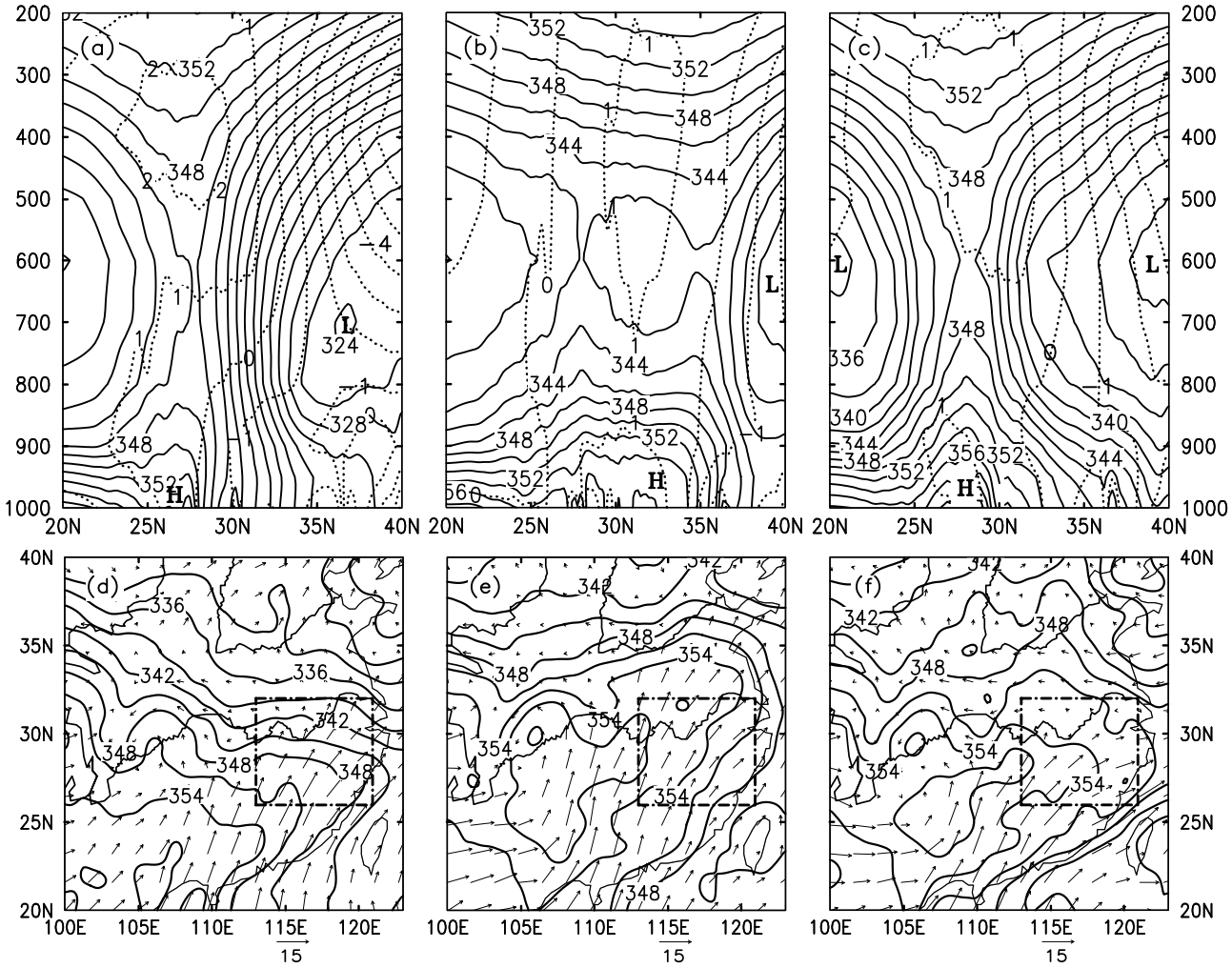

Figure 8. (top) Vertical-latitude cross-section of equivalent potential temperature (θ_e, solid lines, every 2 K) and deviation temperature (dotted lines, every 1°C) zonally averaged across the YRB-ML (i.e., 113–121°E). (bottom) Horizontal distribution of θ_e (contoured at intervals of 3 K) and flow vectors at σ = 0.91: a level that is about 100 hPa above the surface. Both are from the model-domain 1 averaged for the period of (a, d) 12–30 June 1998; (b, e) 1–19 July 1998; and (c, f) 20–31 July 1998.

This weak (mean) extratropical cyclone corresponds to the cyclonic anomaly over the Korean peninsula shown in Figures 2e–2g. MM5 also reproduces more or less another low-pressure system over the SC-GZ-YN area (cf. Figures 3 and 8f). These two cyclonic systems appear to play important roles in determining the magnitudes of the two rainfall centers shown in Figure 3c; this will be explored in detail in a forthcoming study. Clearly, convergence of the northeasterly and southwesterly flows provides necessary lifting of the high-θ_e air for the release of potential instability over the YRB-ML, though much weaker convergence in the northeasterlies. As compared to the first rainy phase, the southwesterly flows over the YRB-ML are weaker and shallower (Figure 9c), which is of typical characteristics of the large-scale mean meridional flow during this period of the summer season. We may speculate that without the northeasterly moisture supply, the relatively weaker southwesterly flows of high-θ_e air would not alone produce the catastrophic rainfall over the YRB-ML.

[29] As one of the major objectives of this study, it is of interest to examine the daily to biweekly rainfall characteristics during the three phases. For this reason, Figure 10 shows Hovmöller diagram, following *Carbone et al.* [2002] and *Zhang et al.* [2003], of the 3-hourly meridionally averaged rainfall rates following the heavy rainfall belts (cf. Figures 3 and 10). Similar observational analyses are also given in order to see to what extent the RCM has reproduced individual rainfall systems associated with the 1998 floods. We have traced the evolution of major rainfall events along the YRB, and found that most of them are associated with organized MCSs. Both the simulation and the observations show a total of 8 well-organized weather systems (i.e., A–H), developing periodically (i.e., every 2–3 days) one after another during the first rainy phase. Evidently, most of the associated MCSs exhibit eastward propagation along the quasi-stationary Meiyu front, with the rainfall amounts maximized as they move across the YRB-ML (Figure 10a). The MCSs are modulated by the large-scale forcings (e.g., WPSH, the Meiyu front, and midlevel

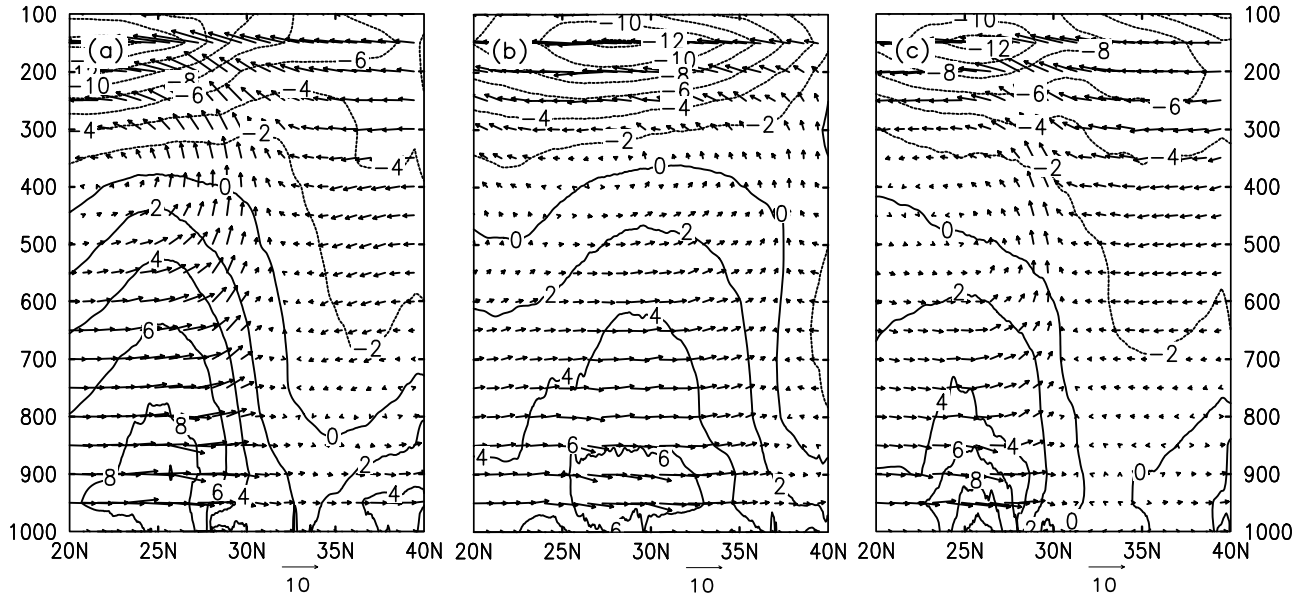

Figure 9. As Figures 8a, 8b, and 8c but for meridional wind speeds (contoured at intervals of 2 m s^{-1}) and in-plane flow vectors. Note that the vertical flow component has been multiplied by 100. Dotted and solid lines refer to northerly and southerly winds, respectively.

traveling waves) and appear to propagate at speeds faster than the synoptic-scale flows; this has also been noted by previous studies [e.g., *Wang et al.*, 2004]. A few locally generated MCSs could also be seen over the YRB-ML after the passages of the eastward propagating MCSs, forming super-MCS complexes (e.g., B and F) that account for sustained precipitation and colder temperatures over the region (cf. Figures 5–7, and 10a and 10c). The increased rainfall and the local development of MCSs are consistent with the channeled moisture supply to the YRB-ML by the monsoonal flows (cf. Figures 2, 8d, and 10a and 10c).

[30] An analysis of the low-level fields reveals the presence of the quasi-stationary low-pressure system over Central China (e.g., see Figure 8d) that provides favorable environments for the intermittent MCS developments and their eastward propagation from the upper to lower reach of the YRB, as depicted by ellipses in Figures 10a and 10c (e.g., B–F). In particular, most of the eastward-propagating MCSs could be traced back to the foothill of Tibet Plateau where favorable topographical lifting occurs (see Figures 4 and 8e) in combination with the local surface heating. That is, deep convection tends to be initiated in the early afternoon, and some could continue until the next morning after an MCS is organized. However, the rainfall amount is small in the upper reach of Yangtze River, and it reaches its peak as moving to the YRB-ML near noon on the next day. The initiation and subsequent evolution of the MCSs are similar to those shown in the study of *Yasunari and Miwa* [2006], so they are not repeated herein. As will be seen later, the diurnal intensity changes at individual locations along Yangtze River could be attributed to the temporal evolution of LLJs that are influenced by the daily surface heating cycle.

[31] As the WPSH progresses northwestward near the end of June 1998, more rainfall begins to appear at the upper reach of Yangtze River (not shown); only two major MCSs (i.e., G and H) move across the YRB-ML despite the presence of similar low-level background flows (cf. Figures 10a and 10c and 8d and 8e). Because of the subsequent dominance of the WPSH over East and Central China, MCSs, developed along the foothill of Tibet Plateau, tend to be suppressed as they move eastward during the transition phase (see Figures 10b and 10d and 3b and 3e). Nevertheless, the heavy rainfall over the upper reach of Yangtze River led to the first and second flood peak at Yichang, HB, on 2 and 17 July, respectively. In contrast, the YRB-ML only experiences a few isolated convective storms as in normal years [*Wang et al.*, 2004]. Near the end of the transition phase (i.e., 17 and 18 July), two organized but non-propagating linear rainfall streaks appear along the YRB, but they are relatively short-lived (Figures 10b and 10d).

[32] Because of the convergent (pronounced) northerly and (weak) southerly high-θ_e air, the second rainy phase is featured with steady convective available potential energy (CAPE) supply from both sides of the shallow Meiyu front that is modulated by diurnal surface processes. The observed rainfall shows two quasi-stationary centers, located near 110°E and 115°E, respectively; heavy rainfall occurred locally at the two locations on a nearly daily basis but at different times (Figure 10b). This steady rainfall period, grouped as the super-MCS-complex I in Figure 10b (and also in Figure 5), lasted for more than 6 days with the highest rate of 457 mm in 3 days (i.e., on 20–22 July) recorded in Wuhan, HB, leading to the third flood peak at Yichang on 24 July. Because of the position errors of the previously mentioned two low-level low-pressure systems (see Figure 8f), the model produces linear non-propagating rainfall streaks with relatively weaker intensity daily along the YRB-ML, namely, a total of 6 streaks during the period of 20–26 July (Figure 10d). On the last two days, both the simulation and observations show two east-propagating rainfall streaks (J)

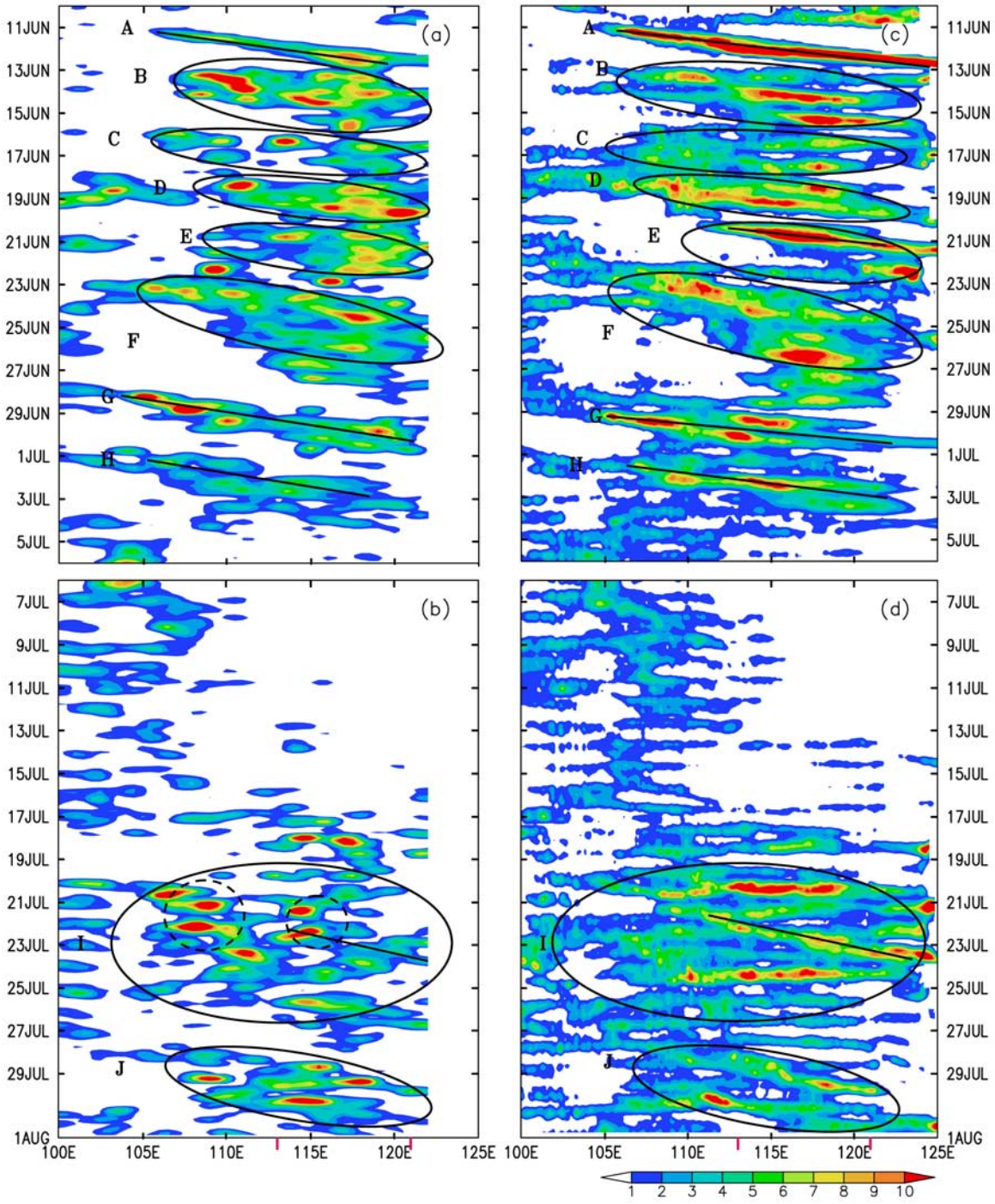

Figure 10. Time-longitude (Hovmöller) diagram of the 3-hourly accumulated rainfall rates [mm (3 hours)$^{-1}$] that are meridionally averaged (i.e., 26–32°N) following the major rainfall belt from (left) the station observations and (right) the model-domain 2 for (a, c) 10 June to 5 July 1998 and (b, d) 6–31 July 1998. Letters "A" to "J" denote major weather systems along the YRB region, and each axis represents single rainfall streak whereas each ellipse represents a series of rainfall events caused by one low-pressure processes. The YRB-ML region is indicated. Local solar time (LST) is used. The two dashed circles refer the two rainfall centers in the second rainy phase.

associated with two MCSs. We believe that MM5 reproduces to some extent the two super-MCS complexes, with one (i.e., J) consisting of propagating MCSs and the other (i.e., I) non-propagating MCSs, but there are marked differences in location and structure of the individual weather systems due to the simulated position errors of the two low-pressure systems.

[33] To see more clearly the diurnal characteristics of rainfall, the temporally and meridionally (i.e., 26–32°N) averaged rainfall across the longitudes of 100–125°E

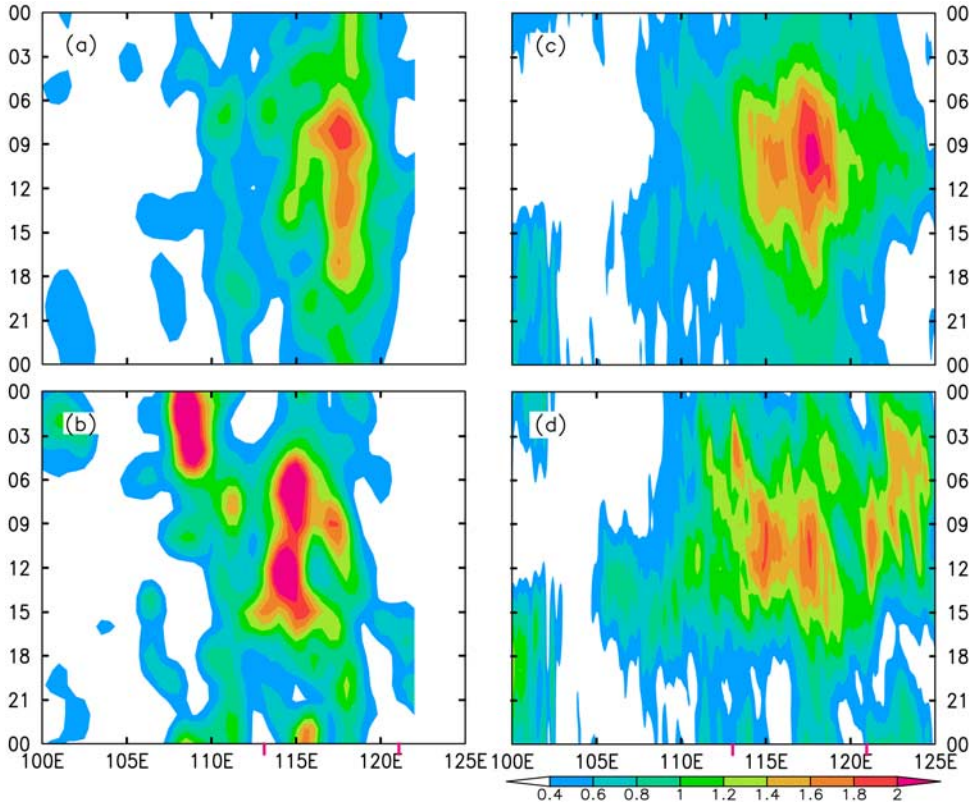

Figure 11. Diurnal variation of the meridionally averaged (27–31°N), hourly rainfall rates (mm hour^{-1}) from (left) the station observations and (right) the model-domain 2 averaged over the YRB-ML during (a, c) 12–30 June 1998 and (b, d) 20–31 July 1998. LST is used.

during each rainy phase is given in Figure 11. Both the simulation and observations show the initiation of deep convection in the afternoon along the foothill of Tibet Plateau during both rainy phases (see Figures 3 and 11). Although Figure 11 shows little evidence of the subsequent downstream propagation due to the use of the temporal and spatial averages with a fixed meridional window, Figures 3 and 10 do reveal continuous rainfall distributed in the anticyclonic monsoonal flows and its eastward propagating characteristics. Of interest is that heavy rainfall tends to occur over the YRB-ML between 0600 and 1200 LST, and 0600 and 1500 LST, during the first and second rainy phases. Because MM5 fails to reproduce the rainfall center near Wuhan, HB, during the second rainy phase (cf. Figures 3c and 3f), a nocturnal rainfall maximum (i.e., occurring between 0000 and 0600 LST) near 108°E is missed (cf. Figures 11b and 11d). Although the peak rainfall rates along YRB-ML are somewhat weaker and wider than the observed, the general rainfall characteristics are reasonably reproduced.

[34] While the initiation of deep convection in the source region could be attributed to the surface heating cycle, the steady rainfall occurring along YRB-ML requires abundant moisture supply into the region in addition to favorable larger-scale conditions [*Yu et al.*, 2007b]. LLJs are persistent features in South China [*Wang, L., et al.*, 2003; and the previous studies suggest the importance of LLJs in determining the Meiyu frontal rainfall over South China [e.g., *Zhai et al.*, 1999; *Xu et al.*, 2001]. However, conventional observations are generally too coarse to capture the temporal and spatial structures of LLJs, so fewer observational studies have been performed to examine the diurnal cycle of LLJs along the YRB [*Wang, L., et al.*, 2003]. For this reason, Figure 12 shows the simulated frequency diagrams of the area-averaged horizontal wind speeds that are peaked at 850 hPa; they are taken slightly to the south of the rainfall belts. Some diurnal variations of horizontal winds are evident to the east of 110°E, with greater amplitudes over the YRB-ML. Of importance is that the LLJs have their peak magnitudes near 0600 LST in both phases, which is about 3–6 hours earlier than the time of heavy rainfall (cf. Figures 11c and 11d and 12). Our preliminary analysis of the model-simulated results indicates that the LLJs are closely related to the eastward propagation of midlevel disturbances that are enhanced by latent heat release. *Xu et al.* [2001], *Zhang and Lu* [2006] also find this feature through case studies of the Meiyu-frontal rainfall. More detailed analysis will be given in our future studies.

[35] As revealed by Figures 8d–8f, the LLJs extend from SCS to the Meiyu frontal zone with a width of 800–1000 km. It follows that the larger-scale circulations play an important role in determining the location and intensity of rainfall along the Meiyu front through the moisture supply by LLJs. It should be mentioned that although the LLJs have an averaged maximum amplitude of 13–14 m s^{-1}, some observed LLJ events were as strong as 30 m s^{-1} (e.g.,

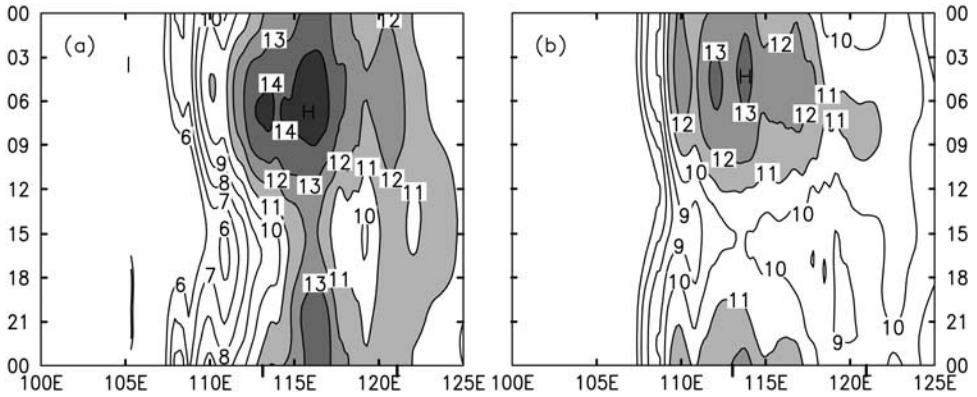

Figure 12. As in Figure 11 but for the 850-hPa horizontal wind speeds (larger than 6 m s^{-1} is contoured at intervals of 1 m s^{-1}) that are meridionally averaged within the range of 25–28°N for (a) 12–30 June 1998 and (b) 20–31 July 1998. LST is used. The wind speed larger than 11 m s^{-1} is shaded.

one occurred on 30 June) during the first rainy phase, and about 20 m s^{-1} during the second phase.

6. Summary and Concluding Remarks

[36] In this study, the daily to submonthly weather and climate characteristics of the extreme rainfall over the YRB-ML during the summer of 1998 are examined using the NCEP/DOE R-2 reanalysis and a 54-day RCM (i.e., MM5) simulation of the associated MCSs with the finest resolution of 4 km. It is shown that the RCM reproduces reasonably well the accumulated rainfall in both distribution and magnitude during the two different Meiyu rainy phases and a transition phase between, the origin of some MCSs along the foothill of Tibet Plateau, their subsequent eastward propagation along the Meiyu front, and the time series of the area-averaged heavy rainfall rates and surface temperature over the YRB-ML, as verified against the R-2 analysis and station observations. In particular, the model simulates the total accumulated rainfall and its associated major MCS events along the YRB-ML during the second rainy phase with weak, shallow Meiyu frontal structures.

[37] It is found that the strength and position of the WPSH and the distribution of the Meiyu front control the general areas of rain production, while the low-level moisture supply through LLJs and cyclonic flows in the Korean peninsula determines whether or not sustaining flooding rain would occur and what rainfall characteristics are at the daily to biweekly timescales during the summer of 1998. Local topography and surface fluxes appear to modulate the rainfall structures and intensities, and likely assist the initiation of deep convection. Results show that the biweekly averaged larger-scale circulations during the first rainy phase resemble in many aspects those occurring in normal years, except for a moister-than-climate state and stronger-than-normal monsoonal flows in Southeast China, whereas the second rainy phase exhibits two abnormal height anomalies in the deep troposphere, i.e., negative over the Korean peninsula and positive over SCS, that favor the convergence of subtropical high-θ air and moist air from the northeast toward the YRB-ML. The model-simulated results indicate that the Meiyu front weakens in depth and intensity as it migrates northward across and then retreats to the YRB-ML, suggesting its decreasing roles in generating the daily to biweekly rainfall over the region. The submonthly Meiyu frontal structures are not well-defined, making the dominant MCS rainfall events less reproducible by RCMs during the second rainy phase. Deficiencies in the cumulus parameterization scheme and its interaction with the grid-scale explicit scheme would also affect the simulated rainfall results during this rainy phase.

[38] Because of the different frontal and larger-scale interactions, the first rainy phase exhibits mostly the eastward propagation of rainfall streaks with the intensity increasing toward the YRB-ML, whereas non-propagating rainfall streaks with diurnal variations tend to occur during the second phase. In both phases, some MCSs are locally developed after the passage or development of a major rainfall system, leading to steady heavy rainfall over the YRB-ML, referred to as the super-MCS complex herein. An analysis of the model-simulated daily weather maps indicates that the former is closely related to the propagation of midlevel mesoscale disturbances that are enhanced by latent heat release, while the latter is more or less dominated by the above-mentioned two quasi-stationary cyclonic systems in Southwest and Northeast China, respectively. The northeasterly moisture supply from the northeastern cyclone over the Korean peninsula appears to play an important role in enhancing the production of steady heavy rain over the YRB-ML during the second rainy phase.

[39] Despite the different daily rainfall characteristics, both the simulation and observations show similar diurnal variations of rainfall during both rainy phases. It is found that the LLJ cores with an average width of 800–1000 km, that are located some distance upstream, occur nearly 3–6 hours in advance of the heavy rainfall over the YRB-ML. This result, if it could be further confirmed by more RCM case studies, could be useful to weather forecasters for their prediction of the timing and location of heavy rainfall along the Meiyu front. Of course, the relationship between the LLJs, the Meiyu front and larger-scale disturbances would differ from case to case during the 1998 floods, as could be seen from Figures 8–10, depending on their relative intensities and locations. This will be the subject of our future study examining different roles of the above features in generating various daily to biweekly rainfall

characteristic during the two rainy phases using the model-simulated data. Sensitivity of the simulated rainfall to cloud and PBL parameterizations as well as surface moisture fluxes at the biweekly to monthly timescales will also be examined.

[40] **Acknowledgments.** This work was supported by the Natural Science Foundation of China grant 40475044 and NSF grant ATM-0342363. The computations were performed at the Department of Atmospheric and Oceanic Science, University of Maryland, and on the Lenovo DeepComp 1800 Supercomputer in LASG of Institute of Atmospheric Physics, Chinese Academy of Sciences.

References

Bei, N., and S. Zhao (2002), Mesoscale analysis of severe local heavy rainfall during the second stage of the 1998 Meiyu season (in Chinese), *Chin. J. Atmos. Sci.*, *26*, 526–540.

Carbone, R. E., J. D. Tuttle, D. A. Ahijevych, and S. B. Trier (2002), Inferences of predictability associated with warm season precipitation episodes, *J. Atmos. Sci.*, *59*, 2033–2056.

Chen, L. (2001), The role of the anomalous snow cover over the Qinghai-Xizang Plateau and ENSO in the great floods of 1998 in the Changjiang River Valley (in Chinese), *Chin. J. Atmos. Sci.*, *25*, 184–192.

Chen, F., and J. Dudhia (2001a), Coupling an advanced land surface-hydrology model with the Penn State-NCAR MM5 modeling system. part I: Model implementation and sensitivity, *Mon. Weather Rev.*, *129*, 569–585.

Chen, F., and J. Dudhia (2001b), Coupling an advanced land surface-hydrology model with the Penn State-NCAR MM5 modeling system. part II: Preliminary model validation, *Mon. Weather Rev.*, *129*, 587–604.

Chen, D., et al. (1998), Annual Report of 1998 Water Conditions (in Chinese), China Water Power Press, Beijing, China. (Available at http://www.chinawater.net.cn/books/98water/)

Dickinson, R. E., A. Henderson-Sellers, and P. J. Kennedy (1993), Biosphere-atmosphere transfer scheme (BATS) version 1 as coupled to the NCAR Community Climate Model, *NCAR Tech. Note NCAR/TN-387+STR*, 72 pp., National Center for Atmospheric Research, Boulder, Colo.

Ding, Y. (1994), *Monsoons over China*, 419 pp., Kluwer Academic Publisher, Dordrecht, Netherlands.

Ding, Y., and G. Hu (2003), A study on water vapor budget over China during the 1998 severe flood periods (in Chinese), *Acta Meteorol. Sinica*, *61*, 129–145.

Dudhia, J. (1989), Numerical study of convection observed during the winter monsoon experiment using a mesoscale two-dimensional model, *J. Atmos. Sci.*, *46*, 3077–3107.

Gao, X., Y. Xu, Z. Zhao, J. S. Pal, and F. Giorgi (2006), Impacts of horizontal resolution and topography on the numerical simulation of East Asian precipitation (in Chinese), *Chin. J. Atmos. Sci.*, *30*, 185–192.

Giorgi, F. (1990), Simulation of regional climate using a limited area model nested in a general circulation model, *J. Clim.*, *3*, 941–963.

Huang, R., Y. Xu, P. Wang, and L. Zhou (1998), The features of the catastrophic flood over the Changjiang River Basin during the summer of 1998 and cause exploration (in Chinese), *Clim. Environ. Res.*, *3*, 300–312.

Janjić, Z. I. (1994), The step-mountain eta coordinate model: Further developments of the convection, viscous sublayer, and turbulence closure schemes, *Mon. Weather Rev.*, *122*, 927–945.

Kain, J. S. (2004), The Kain-Fritsch convective parameterization: An update, *J. Appl. Meteorol.*, *43*, 170–181.

Lau, K.-M., and H. Weng (2001), Coherent modes of global SST and summer rainfall over China: An assessment of the regional impacts of the 1997–1998 El Niño, *J. Clim.*, *14*, 1294–1308.

Lee, D. K., D. H. Cha, and H. S. Kang (2004), Regional climate simulation of the 1998 summer flood over East Asia, *J. Meteorol. Soc. Jpn.*, *82*, 1735–1753.

Leung, L. R., S. Zhong, Y. Qian, and Y. Liu (2004), Evaluation of regional climate simulations of the 1998 and 1999 East Asian summer monsoon using the GAME/HUBEX observation data, *J. Meteorol. Soc. Jpn.*, *82*, 1695–1713.

Qian, J.-H., W.-K. Tao, and K.-M. Lau (2004), Mechanisms for torrential rain associated with the Mei-yu development during SCSMEX 1998, *Mon. Weather Rev.*, *132*, 2–27.

Ren, R., and G. Wu (2003), On the short-term structure and formation of the subtropical anticyclone in the summer of 1998 (in Chinese), *Acta Meteorol. Sin.*, *61*, 180–195.

Ren, R., Y. Liu, and G. Wu (2004), On the short-term variation of subtropical anticyclone over the Western Pacific affected by the mid-high latitudes circulation in July 1998 (in Chinese), *Chin. J. Atmos. Sci.*, *28*, 571–578.

Ren, R., Y. Liu, and G. Wu (2007), Impact of South Asia High on the short-term variation of the subtropical anticyclone over western Pacific in July 1998 (in Chinese), *Acta Meteorol. Sin.*, *65*, 183–197.

Reynolds, R. W., and T. M. Smith (1994), Improved global sea surface temperature analyses using optimum interpolation, *J. Clim.*, *7*, 929–948.

Sun, J., and S. Zhao (2003), A study of special circulation during Meiyu season of the Yangtze River Basin in 1998 (in Chinese), *Clim. Environ. Res.*, *8*, 291–306.

Sun, S., and S. Ma (2001), A study on the relationship between the anomaly of subtropical high over the Western Pacific and the heavy flooding in Yangtze River Valley in 1998 (in Chinese), *Acta Meteorol. Sin.*, *59*, 719–729.

Tang, J., M. Zhao, and B. Su (2006), Effects of model resolution on the simulation of regionally climatic extreme events (in Chinese), *Acta Meteorol. Sin.*, *64*, 432–442.

Tao, S., Q. Zhang, and S. Zhang (1998), The great floods in the Changjiang River Valley in 1998 (in Chinese), *Clim. Environ. Res.*, *3*, 290–299.

Wang, L., W.-L. Zhang, and J. Zhou (2003), Statistic analysis on the south-westerly LLJ in China (in Chinese), *J. Nanjing Inst. Meteorol.*, *26*, 797–805.

Wang, Y.-Q., O. L. Sen, and B. Wang (2003), A highly resolved regional climate model (IPRC-RegCM) and its simulation of the 1998 severe precipitation event over China. part I: Model description and verification of simulation, *J. Clim.*, *16*, 1721–1738.

Wang, C.-C., G. T.-J. Chen, and R. E. Carbone (2004), A climatology of warm-season cloud patterns over East Asia based on GMS infrared brightness temperature observations, *Mon. Weather Rev.*, *132*, 1606–1629.

Xu, H., J. He, and B. Zhou (2001), Common features of synoptic systems related to heavy rainstorms in the middle Changjiang River Basin during summer (in Chinese), *Q. J. Appl. Meteorol.*, *12*, 317–326.

Xue, Y., R. Vasic, Z. Janjic, F. Mesinger, and K. E. Mitchell (2007), Assessment of dynamic downscaling of the continental U.S. regional climate using the Eta/SSiB Regional Climate Model, *J. Clim.*, *20*, 4172–4193.

Yasunari, T., and T. Miwa (2006), Convective cloud systems over the Tibetan Plateau and their impact on meso-scale disturbances in the Meiyu/Baiu frontal zone: A case study in 1998, *J. Meteorol. Soc. Jpn.*, *84*, 783–803.

Yu, R., T. Zhou, A. Xiong, Y. Zhu, and J. Li (2007a), Diurnal variations of summer precipitation over contiguous China, *Geophys. Res. Lett.*, *34*, L01704, doi:10.1029/2006GL028129.

Yu, R., Y. Xu, T. Zhou, and J. Li (2007b), Relation between rainfall duration and diurnal variation in the warm season precipitation over central eastern China, *Geophys. Res. Lett.*, *34*, L13703, doi:10.1029/2007GL030315.

Zhai, G., H. Ding, S. Sun, and K. Gao (1999), Physical characteristics of heavy rainfall associated with strong low level jet (in Chinese), *Chin. J. Atmos. Sci.*, *23*, 112–118.

Zhang, D.-L. (1989), The effect of parameterized ice microphysics on the simulation of vortex circulation with a mesoscale hydrostatic model, *Tellus*, *41A*, 132–147.

Zhang, X. F., and H. C. Lu (2006), Analysis of latent heat and its feedback mechanism during a Meiyu-front rainstorm (in Chinese), *Meteorol. Sci. Technol.*, *34*, 567–573.

Zhang, D.-L., W. Zheng, and Y.-K. Xue (2003), A numerical study of early summer regional climate and weather over the LSA-East. part I: Model implementation and verification, *Mon. Weather Rev.*, *131*, 1895–1909.

Zhang, X., S. Tao, and Q. Zhang (2002), An analysis on development of meso-β convective system along Meiyu front associated with flood in Wuhan in 20–21 July 1998 (in Chinese), *J. Appl. Meteorol. Sci.*, *13*, 385–397.

H. Liu and B. Wang, LASG, Institute of Atmospheric Physics, Chinese Academy of Sciences, No. 40 Huayanli, Chaoyang District, Beijing 100029, China.

D.-L. Zhang, Department of Atmospheric and Oceanic Science, University of Maryland, College Park, MD 20742-2425, USA. (dalin@atmos.umd.edu)